

Birck Nanotechnology Center

Other Nanotechnology Publications

Purdue Libraries

Year 2004

The discretized Schroedinger equation
and simple models for semiconductor
quantum wells

Timothy B. Boykin*

Gerhard Klimeck†

*The University of Alabama, Huntsville,

†Purdue University - Main Campus, gekco@ecn.purdue.edu

This paper is posted at Purdue e-Pubs.

<http://docs.lib.purdue.edu/nanodocs/121>

The discretized Schrödinger equation and simple models for semiconductor quantum wells

Timothy B Boykin¹ and Gerhard Klimeck^{2,3}

¹ Department of Electrical and Computer Engineering, The University of Alabama in Huntsville, Huntsville, AL 35899, USA

² Jet Propulsion Laboratory, California Institute of Technology, 4800 Oak Grove Road, MS 169-315, Pasadena, CA 91109, USA

³ Network for Computational Nanotechnology, School of Electrical and Computer Engineering, Purdue University, West Lafayette, IN 47907, USA

Received 23 March 2004

Published 4 May 2004

Online at stacks.iop.org/EJP/25/503

DOI: 10.1088/0143-0807/25/4/006

Abstract

The discretized Schrödinger equation is one of the most commonly employed methods for solving one-dimensional quantum mechanics problems on the computer, yet many of its characteristics remain poorly understood. The differences with the continuous Schrödinger equation are generally viewed as shortcomings of the discrete model and are typically described in purely mathematical terms. This is unfortunate since the discretized equation is more productively viewed from the perspective of solid-state physics, which naturally links the discrete model to realistic semiconductor quantum wells and nanoelectronic devices. While the relationship between the discrete model and a one-dimensional tight-binding model has been known for some time, the fact that the discrete Schrödinger equation admits analytic solutions for quantum wells has gone unnoted. Here we present a solution to this new analytically solvable problem. We show that the differences between the discrete and continuous models are due to their fundamentally different bandstructures, and present evidence for our belief that the discrete model is the more physically reasonable one.

1. Introduction

It is well known that the Schrödinger equation, even in one dimension, admits precious few analytic solutions, so that most interesting problems must be solved numerically. The availability of relatively powerful, inexpensive computers along with simple programming languages and numerical packages has naturally led to the increasing assignment of computer problems in undergraduate and beginning graduate quantum mechanics classes. When

introduced in this context, the one-dimensional discrete Schrödinger equation is often presented as the inferior numerical approximation to the ‘true’ continuous equation, exact only in the limit of infinitesimal lattice spacing. While this position is mathematically precise, it ignores a far deeper question: ‘Is the continuous Schrödinger equation the most physically reasonable choice for realistic modelling of semiconductor quantum wells and other nanoelectronic devices?’

It is our assertion that the answer to this question is a resounding ‘no’. In the first place, when applied to semiconductor quantum wells the continuous one-dimensional Schrödinger equation is actually an equation of motion for the wavefunction envelope. As such its solutions are meaningless at length scales below a lattice constant. Hence the finite mesh size of the discrete model is a strength, not a weakness. Second, the $E(k)$ dispersion for a bulk semiconductor more closely resembles that of the discrete model than it does the parabola of the continuous model, since the parabolic dispersion is in fact only accurate for energies in the neighbourhood of an extremum. The discrete model therefore incorporates much more of the actual physics of semiconductor crystals than does the continuous model. This is no accident: the more realistic physics of the discrete Schrödinger equation arises from its equivalence to a tight-binding model for a crystalline solid [1], in both the bulk (periodic potential) and quantum-confined cases.

While the relationship between the tight-binding model and the discrete Schrödinger equation has been known for some time for the bulk case, its consequences and implications for the quantum-confined case (e.g., the infinite square well) have been far less well appreciated. This is perhaps due to the fact that to date analytic solutions for tight-binding models of quantum wells have not been presented, to our knowledge.

Analytic solutions are especially important for problems which serve as the starting point for detailed numerical calculations, since they help clarify the physics of the predicted behaviour. Without analytic results to serve as guides it is often difficult to correctly interpret purely numerical results. The infinite square well serves as just such a starting point for both continuous and discrete calculations. The analytic solutions of the continuous model have long been used to estimate the importance of various perturbing potentials. Analytic solutions of the discrete model could be employed in a similarly profitable manner.

Here we present a new analytically solvable quantum mechanics problem—the discrete version of the infinite square well—and show how its solutions display the bandstructure imposed by the discretization itself, due to its equivalence to a tight-binding chain. The effort required to find an eigenstate in the analytic method for the discrete model is independent of the quantum well width unlike its numerical treatment. To set the stage, we briefly restate the relationship of the solutions for the tight-binding chain in bulk to the continuous, free-particle Schrödinger equation. Next, we derive and discuss the exact solution of the infinite square well for the discrete case, showing how the bandstructure of the tight-binding model leads to very different physics for the discrete versus the continuous infinite square well model.

2. Continuous and discrete Schrödinger equations

2.1. General

Simple time-independent quantum-mechanical models are based upon the one-dimensional time-independent Schrödinger equation

$$-\frac{\hbar^2}{2m^*} \frac{d^2\psi}{dz^2} + U(z)\psi(z) = E\psi(z). \quad (1)$$

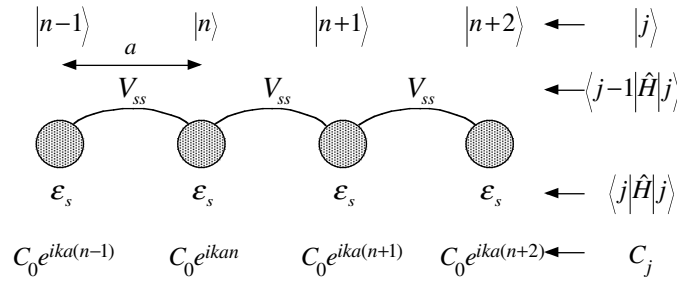


Figure 1. Segment of a chain of atoms, each with one s-like orbital; the lattice spacing is a . The kets (one orbital per atom) are listed at the top, followed by the nearest-neighbour (or ‘hopping’) matrix element, V_{ss} . The third row shows the onsite matrix element for each orbital, ϵ_s . The last row shows the wavefunction coefficients for a bulk chain (one to which periodic boundary conditions have been applied).

For modelling truly free particles the mass m^* is taken to be the actual mass and ψ the full wavefunction; for modelling electrons or holes in semiconductors, m^* represents the effective mass and ψ the envelope of the wavefunction. Regardless of the specific interpretation, equation (1) is what senior undergraduate and beginning graduate students first encounter in quantum mechanics class. Equation (1) must be solved numerically for all but the simplest potentials, U . This is easily accomplished by discretizing it using the standard central-difference formula for the second derivative,

$$\frac{d^2\psi}{dz^2} \approx \frac{1}{a^2}[\psi(z-a) - 2\psi(z) + \psi(z+a)] \quad (2)$$

and evaluating the functions and derivatives at points $z_j = ja$,

$$\left(-\frac{\hbar^2}{2m^*a^2}\right)\psi_{j-1} + \left[\frac{\hbar^2}{m^*a^2} + U_j - E\right]\psi_j + \left(-\frac{\hbar^2}{2m^*a^2}\right)\psi_{j+1} = 0 \quad (3)$$

where $U_n = U(z_n)$, $\psi_n = \psi(z_n)$. In the finite-difference method, equation (3) is one row of the tridiagonal matrix eigenvalue equation.

Equation (3) contains more than mere mathematics, for it is essentially the tight-binding approximation applied to a chain of atoms with spacing a and one orbital per atom [1]. This chain of atoms along with its Hamiltonian matrix elements is illustrated in figure 1 for the bulk case ($U = 0$). Each atom in the chain has one s-orbital, which is taken to be orthogonal to orbitals on other atoms. For a Hamiltonian which couples only nearest-neighbour orbitals the matrix elements are

$$\langle s; j'a | \hat{H} | s; ja \rangle = [\epsilon_s + U_j]\delta_{j',j} + V_{ss}[\delta_{j',j+1} + \delta_{j',j-1}] \quad (4)$$

where $|s; na\rangle$ denotes an s-orbital on the atom located at na and the Hamiltonian is written as $\hat{H} = \hat{H}_0 + \hat{U}$:

$$\langle s; j'a | \hat{H}_0 | s; ja \rangle = \epsilon_s\delta_{j',j} + V_{ss}[\delta_{j',j+1} + \delta_{j',j-1}] \quad (5)$$

$$\langle s; j'a | \hat{U} | s; ja \rangle = U_j\delta_{j',j}. \quad (6)$$

Note that \hat{H}_0 includes the periodic potential of the chain of atoms. In this basis the wavefunction is

$$|\psi\rangle = \sum_j C_j |s; ja\rangle \quad (7)$$

so that the Schrödinger equation appears as a tridiagonal matrix eigenvalue equation with rows:

$$\langle s; na | [\hat{H} - \hat{1}E] | \psi \rangle = V_{ss}C_{n-1} + [\varepsilon_s + U_n - E]C_n + V_{ss}C_{n+1} = 0. \quad (8)$$

Comparing equations (3) and (8) shows that they are identical provided that the parameters satisfy

$$V_{ss} = -\frac{\hbar^2}{2m^*a^2} \quad \varepsilon_s = \frac{\hbar^2}{m^*a^2}. \quad (9)$$

Note that the negative sign on the nearest-neighbour parameter V_{ss} makes sense, as the true inter-atomic potential included in \hat{H}_0 will be negative (roughly coulomb-like).

2.2. Bulk models: free particles versus discrete periodicity

In bulk ($U = 0$) equations (1) and (8) have different eigenstates and dispersions. Equation (1), the continuous Schrödinger equation, has plane-wave solutions $\psi(z) = \exp(ikz)/\sqrt{B}$, for convenience normalized to a length B , with parabolic dispersion

$$E(k) = \frac{\hbar^2 k^2}{2m^*} \quad (10)$$

due to conservation of true momentum. On the other hand, invoking Bloch's theorem and applying periodic boundary conditions $C_{j+2M} = C_j$ to equation (7) over a length $B = 2Ma$, where $2M$ is the number of atoms, results in a dispersion

$$E(k) = \varepsilon_s + 2V_{ss} \cos(ka) \quad (11)$$

and wavefunction coefficients

$$C_j(k) = \frac{1}{\sqrt{2M}} e^{ikja} \quad k = \frac{2n\pi}{2Ma} \quad n = -(M-1), \dots, -1, 0, 1, \dots, (M-1), M \quad (12)$$

where the index j runs over $2M$ consecutive values and the starting index is of course arbitrary (as it merely gives an overall phase). For any realistic bulk model $M \gg 1$ and thus k is effectively continuous in the range $-\pi/a < k \leq \pi/a$. The coefficient equations (12) come from the propagation factors (see the appendix).

Equations (9)–(11) show that the two models agree only in the small- k limit, near the minimum. Figure 2 illustrates a comparison between equation (11) for $\varepsilon_s = 2.0$ eV, $V_{ss} = -1.0$ eV and equation (10) for m^* computed from equation (9) corresponding to these ε_s and V_{ss} . While the continuous and discrete dispersions agree near the minimum, the most striking differences between the two are the periodicity and finite bandwidth of the discrete dispersion on the one hand, and the aperiodic nature and unbounded bandwidth of the continuous dispersion on the other hand. These characteristics reflect the discrete translational symmetry and finite nearest-neighbour coupling of the tight-binding model and the continuous translational symmetry of the continuous model. These dramatically different bulk dispersions result in profoundly different bound-state spectra as described in the next subsection.

2.3. The infinite square well: continuous and discrete models

In an infinite quantum well the boundary conditions of both models require that the eigenstates be linear combinations of the bulk states; only certain discrete wavevectors from the bulk (quasi-) continuum are allowed. Different underling $E(k)$ dispersions will, therefore, directly

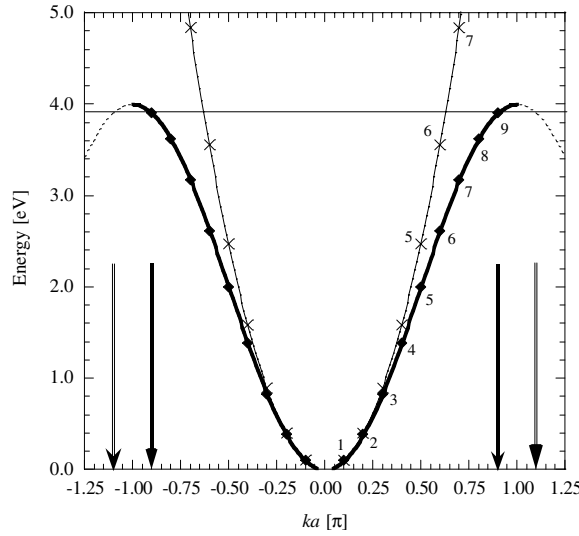


Figure 2. Bandstructures or $E(k)$ dispersions for the atomic chain of figure 1 and the continuous Schrödinger equation along with bound state energies for a well of nine sites ($N = 4$) or length $L = 10a$. The continuous model is graphed with the thin solid parabola; the discrete model with the cosine, heavy solid in the first Brillouin zone and dotted outside it. The parameters of the tight-binding model are $\varepsilon_s = 2.0$ eV, $V_{ss} = -1.0$ eV; the effective mass of the continuous model is consistent with these values. The Bloch states contributing to each bound state are indicated by symbols (discrete: diamonds, continuous: crosses) and the positive- k Bloch states are labelled by the indices of the bound states to which they contribute. Solid arrows indicate the phases of the two Bloch states making up the bound state: $\exp(\pm ika)$, $ka = 0.9\pi$. Due to the periodicity of the dispersion states with $|ka| > \pi$ (i.e., falling outside the first Brillouin zone) are not unique, as shown by the double arrows.

impact the bound spectra. For the continuous case of an infinite square well with barriers at $z = \pm L/2$ ($U = 0$, $|z| < L/2$), the eigenvalues and eigenfunctions are the familiar [2],

$$E_n = \frac{n^2 \pi^2 \hbar^2}{2m^* L^2} = \frac{\hbar^2 k_n^2}{2m^*} \quad n = 1, 2, 3, \dots \quad k_n \doteq \frac{n\pi}{L} \quad (13)$$

$$\psi_{2j+1}(z) = \sqrt{\frac{2}{L}} \cos(k_{2j+1}z) \quad j = 0, 1, 2, \dots \quad |z| \leq \frac{L}{2} \quad (14)$$

$$\psi_{2j}(z) = \sqrt{\frac{2}{L}} \sin(k_{2j}z) \quad j = 1, 2, \dots \quad |z| \leq \frac{L}{2} \quad (15)$$

where due to the symmetry of the Hamiltonian the eigenstates are simultaneous parity eigenstates. The wavefunctions, equations (14) and (15), of course vanish at the points $z = \pm L/2$.

In the discrete case the proper description of the boundary conditions is somewhat subtle. As shown in the appendix, the boundary conditions can be rigorously derived by taking the limit that the confining potential in the barriers $U \rightarrow \infty$, but the derivation is more complicated than in the continuous case, requiring the solution of the forward- and reverse propagation constants [3]. In either case, the most helpful description is that of the perfect confinement, namely, the wavefunction vanishes outside the quantum well. Consider a quantum well (in which $U = 0$) which comprises a total $2N + 1$ sites, indexed by $j = -N, -(N - 1), \dots, N - 1, N$. Figure 3 illustrates this chain. The atoms at $\pm(N + 1)$ are empty to indicate that the

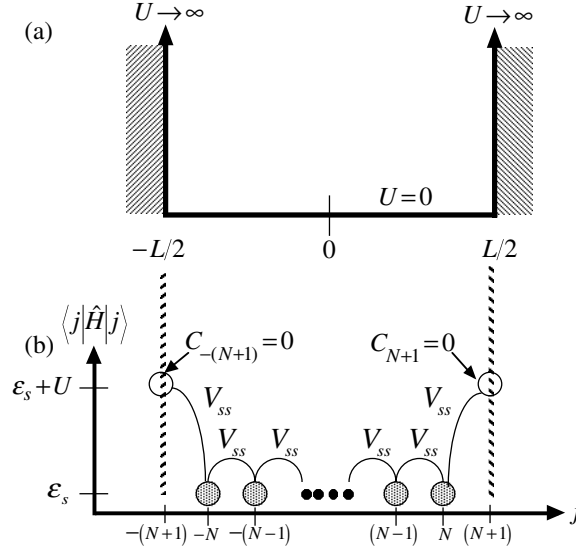


Figure 3. Infinite square well in the continuous (a) and tight-binding (b) models. In the tight-binding model the on-site energies are graphed on the vertical axis; the horizontal axis shows atom locations. Nearest-neighbour couplings are shown as links between atoms. Shaded atoms are in the well, white atoms in the barriers. The confining energy is taken as a limit $U \rightarrow \infty$ as discussed in the appendix. Orbitals with indices $-N \leq j \leq N$ (shaded) have nonzero expansion coefficients; the wavefunction vanishes at those for $j = \pm(N+1)$ (empty), as shown explicitly by $C_{\pm(N+1)} = 0$.

wavefunction vanishes on these sites, decoupling them from the atoms in the well. The wavefunctions (7) are then

$$|\psi_n\rangle = \sum_{j=-(N+1)}^{N+1} C_j^{(n)} |s; ja\rangle \quad n = 1, 2, \dots, 2N+1 \quad (16)$$

and perfect confinement requires that

$$C_{-(N+1)}^{(n)} = C_{N+1}^{(n)} = 0. \quad (17)$$

Note that we can place no further requirements on the coefficients beyond the sites $\pm(N+1)$: this is exactly analogous to the condition that the continuous wavefunction, equations (14) and (15) vanish at $z = \pm L/2$.

One difference with the continuous case immediately stands out: there are exactly $2N+1$ eigenfunctions, equation (16), not an infinite number as in equations (14) and (15). This fact is easily seen from the perspective of linear algebra (with $2N+1$ atoms and one orbital per atom there are $2N+1$ basis states), and indeed, the Hamiltonian for this structure is the tridiagonal matrix of dimension $2N+1$:

$$H_{QW} = \begin{bmatrix} \varepsilon_s & V_{ss} & 0 & \cdots & \cdots & 0 \\ V_{ss} & \varepsilon_s & V_{ss} & 0 & \cdots & 0 \\ 0 & V_{ss} & \varepsilon_s & V_{ss} & \ddots & \vdots \\ \vdots & \ddots & \ddots & \ddots & \ddots & 0 \\ \vdots & \cdots & 0 & V_{ss} & \varepsilon_s & V_{ss} \\ 0 & \cdots & \cdots & 0 & V_{ss} & \varepsilon_s \end{bmatrix}. \quad (18)$$

More importantly, the finite number of eigenstates also manifests itself in the physics of the problem as we shall see shortly.

The eigenstates may be found without numerical diagonalization of Hamiltonian (18). A simple and attractive argument, rigorously correct for the single-band case considered here and essentially that used in the analytic solution in the continuous model, casts the infinite quantum well as a resonator problem: in a resonator of length L the wavefunction must have a node at each of the boundaries, hence the resonator accommodates only an integral number of half-wavelengths and $k = n\pi/L$, $n = 1, 2, \dots$.

While this description is easily grasped, it glosses over some essential physics, and in fact no longer applies in a multi-band model [4]⁴. The more correct road to the analytic solution involves invoking the principle of superposition. The hard-wall boundary conditions (17) break the discrete translational symmetry of the chain. Thus, even though the potential is constant in the well, a bound eigenstate must be composed of a superposition of all propagating (and, in larger models, evanescent) bulk eigenstates available at the corresponding eigenenergy; these are simultaneous eigenstates of the Hamiltonian and the discrete translation operator (see the appendix). In the single-band case considered here, equation (A.12) shows that the propagation factors for bulk states in the band are $\exp(\pm ika)$. Hence, the coefficients of the bound states are linear combinations of degenerate complex exponentials $\exp(\pm ika_j)$. Since the quantum well is symmetric the coefficients C also must be parity eigenstates:

$$C_j^{(n)} = \sqrt{\frac{1}{N+1}} \begin{cases} \cos(k_n^{(e)} ja) & \text{even states} \\ \sin(k_n^{(o)} ja) & \text{odd states.} \end{cases} \quad (19)$$

The normalization in equation (19) may be found using sums 1.351(1), (2) in [5] and equations (20) and (21).

Each bound state is thus a superposition of discrete allowed bulk states, found by imposing the boundary conditions (17). For the even coefficients this process yields

$$\cos[k_n^{(e)} a(N+1)] = 0 \Rightarrow k_n^{(e)} = k_{2m+1} = \frac{(2m+1)\pi}{2(N+1)a} = \frac{(2m+1)\pi}{L} \quad m = 0, 1, \dots, N \quad (20)$$

while for the odd coefficients it gives

$$\sin[k_n^{(o)} a(N+1)] = 0 \Rightarrow k_n^{(o)} = k_{2m} = \frac{2m\pi}{2(N+1)a} = \frac{2m\pi}{L} \quad m = 1, 2, \dots, N. \quad (21)$$

The restrictions on k in equations (20) and (21) guarantee that equation (8) is satisfied for $n = \pm N$. Note that while the allowed k -values are of the same form as in the continuous case, equations (14) and (15), here they are finite in both number and value. The interpretation $L = 2(N+1)a$ in equations (20) and (21) makes perfect sense, for between the two bounding zeros of the wavefunction at $j = \pm(N+1)$ there are $2(N+1)$ intervals, each of length a . Since the potential is constant in the well, the bound state energies are found by substituting equation (20) or (21) for k into equation (11).

Although the allowed k -values take the same form as in the continuous model ($k = n\pi/L$), the discrete case is fundamentally different, since it has a finite number of eigenstates, $(2N+1)$, and there is a maximum value, $k_{\max} = k_{2N+1} = (2N+1)\pi/L$. Due to the periodic bulk dispersion (11), discrete states described by k outside the specified ranges, equation (20) for even states and equation (21) for odd, are simply phase-shifted versions of states within these

⁴ In a multi-band model the hard-wall boundary conditions generally lead to systems of simultaneous, transcendental equations. For example, in a two-band model one finds a pair of equations for the even states and a pair for the odd states.

ranges. In the language of solid-state physics, such a bound state is made up of bulk states lying outside the first Brillouin zone and therefore is not unique. To see this consider one of the odd states, and instead of choosing one of the allowed k in equation (21), choose

$$k_{2l} = \frac{2l\pi}{2(N+1)a} = \frac{2(N+1+n)\pi}{2(N+1)a} \quad n = 0, 1, 2, \dots, N \quad (22)$$

where $l = N + 1 + n$. The coefficients C for this odd bound state are easily rewritten as

$$C_j(k_{2l}) = \sqrt{\frac{1}{N+1}} \sin \left[2\pi j - \frac{2(N+1-n)\pi}{2(N+1)} j \right] = -\sqrt{\frac{1}{N+1}} \sin \left[\frac{2(N+1-n)\pi}{2(N+1)} j \right]. \quad (23)$$

Omitting the trivial solution $n = 0$, it is clear from equation (23) that the solution for $l = N + 1 + n$ is identical to that for $m = N + 1 - n$, except for a phase.

2.4. Infinite square well: results

In addition to the bulk dispersions, figure 2 illustrates the differences between the continuous and discrete models for bound states. The bulk dispersion of the discrete model is graphed with a heavy solid line inside the first Brillouin zone; outside it is continued briefly with a light dashed line to indicate states which are not unique. Also plotted are the Bloch states contributing to the bound states of a nine-site ($9 = 2N + 1 \Rightarrow L = 2(N + 1)a = 10a$) quantum well. Solid diamonds indicate all nine of these Bloch states for the tight-binding model while crosses indicate the first seven pairs of plane waves for the continuous model; numerals indicate the bound states to which they contribute.

Figure 2 has much to say about these models. As noted above, while the value of k is of course unconstrained for the continuous model, it is restricted to the first Brillouin zone of the tight-binding model since states outside it are not unique. As a specific example, consider the highest bound state in the tight-binding model, labelled 9. The Bloch states contributing to this bound state are indicated with solid arrows at $ka = \pm 0.9\pi$. Since the dispersion is periodic, states related by subtracting or adding 2π to these values, located at $ka = \mp 1.1\pi$ and indicated by double arrows, are redundant. (Solid and double-arrow Bloch states with common arrow heads are the same.)

Beyond the difference in allowed k -values, note that the bound-state energies in the two models show an increasing discrepancy for higher states, $n > 4$. The bound states of the tight-binding model become more closely spaced as their Bloch state components approach the Brillouin zone boundaries. Below we show that this is the expected behaviour when one views the lower states as those of electrons at the bottom of a conduction band and the upper states as holes at the top of a valence band.

According to equation (13), the dispersion of the continuous model is strictly parabolic in the wavevector, k , and hence in the eigenstate index, n . The parabola has positive curvature, characteristic of a free particle of positive mass. In contrast, equation (11) and figure 2 make it clear that the discrete model has approximately parabolic dispersion only near two points, $k = 0, \pi/a$. Near $k = 0$, the second-order Taylor expansion of equation (11) gives

$$E_n - E_{\min} \approx -\frac{V_{ss}\pi^2 n^2}{4(N+1)^2} = \frac{|V_{ss}|\pi^2 n^2 a^2}{L^2} \quad (24)$$

where the index, n , is small, $E_{\min} = E(0) = \varepsilon_s + 2V_{ss}$ is the energy of the band minimum, and as discussed above, $L = 2(N + 1)a$. With V_{ss} given by equation (9), equation (24) agrees

with equation (13). Near $k = \pi/a$ the second-order Taylor expansion has negative curvature ($V_{ss} < 0$):

$$E(k) \approx \varepsilon_s - 2V_{ss} + V_{ss}a^2 \left(k - \frac{\pi}{a}\right)^2. \quad (25)$$

Bound states at energies in the vicinity of the band maximum, $E_{\max} = E(\pi/a) = \varepsilon_s - 2V_{ss}$, therefore behave like valence-band bound states in semiconductor quantum wells. These states are, in other words, hole-like. This behaviour becomes clear when the index in equations (20) and (21) is replaced by an offset from the maximum bound state, $m = N - n'$ and the resulting k substituted into equation (25)

$$E_{\max} - E_{m'} \approx -\frac{V_{ss}\pi^2 m'^2}{4(N+1)^2} = \frac{|V_{ss}|\pi^2 m'^2 a^2}{L^2} \quad (26)$$

where $m' = (2n' + 1)$, $n' = 0, 1, \dots, N$ for even states and $m' = 2(n' + 1)$, $n' = 0, 1, \dots, N - 1$ for odd states. Thus adjacent bound state energies become increasingly separated as the energy below E_{\max} increases, behaviour characteristic of holes.

As shown above, both $E_n - E_{\min} \approx |V_{ss}|\pi^2 n^2 a^2 / L^2$ for electron states and $E_{\max} - E_{m'} \approx |V_{ss}|\pi^2 m'^2 a^2 / L^2$ for hole states, which suggests a relationship between corresponding states: this is precisely the case. For the quantum well with $2N + 1$ sites the relationship between even states 1 and $2N + 1$ is

$$C_j^{(2N+1)} = \sqrt{\frac{1}{N+1}} \cos \left[\frac{j\pi(2N+1)}{2(N+1)} \right] = \sqrt{\frac{1}{N+1}} \cos \left[j\pi - \frac{j\pi}{2(N+1)} \right] = (-1)^j C_j^{(1)}. \quad (27)$$

The argument of the second cosine in equation (27) shows that the first hole state is indeed measured with respect to the Brillouin zone face at $k = \pi/a$. Thus, in the tight-binding model, the envelope of state $2N + 1$ consists of that of state 1 amplitude-modulating fast oscillations characterized by $k = \pi/a$. This further reinforces the connection between the electron-state and hole-state viewpoints. In the case of an even number of sites, analysis of the coefficients as above shows that states 1 and $2N$ have the same probability density, but opposite parity, unlike the case of an odd number of sites.

Wavefunction results for the tight-binding model illustrate these two viewpoints vividly as well as differences between the tight-binding and continuous models. Figure 4 graphs probability densities of states 1 and 9 in the continuous and tight-binding models. In the continuous model, the probability density $|\psi_n(z)|^2$ is defined throughout the well and is plotted with solid (state 1) and dotted (state 9) lines. As expected, there is one peak for state 1 while state 9 has nine peaks. In the tight-binding model, the probability density $|C_j^{(n)}|^2$ is defined only at the atomic sites and is indicated by solid diamonds (state 1) and open circles (state 9). As expected from equation (27), these densities of the electron-like and hole-like quantum well ground states coincide exactly.

The foregoing discussion only touches on the technological importance of the discretized Schrödinger equation and its tight-binding equivalent in terms of modelling heterostructures such as quantum wells, wires and dots. The tight-binding treatment is well suited to these devices since it allows for atomic-level resolution of interfaces and surfaces and provides a straightforward means for incorporating applied potentials. Frensley [6] gives an accessible treatment of the open boundary conditions for various devices (especially tunnelling devices). A more advanced treatment of non-equilibrium transport can be found in [7]. More complete, multi-band tight-binding models are needed to accurately include many-valley and many-band effects, often requiring special numerical methods (see [3, 8, and 9]).

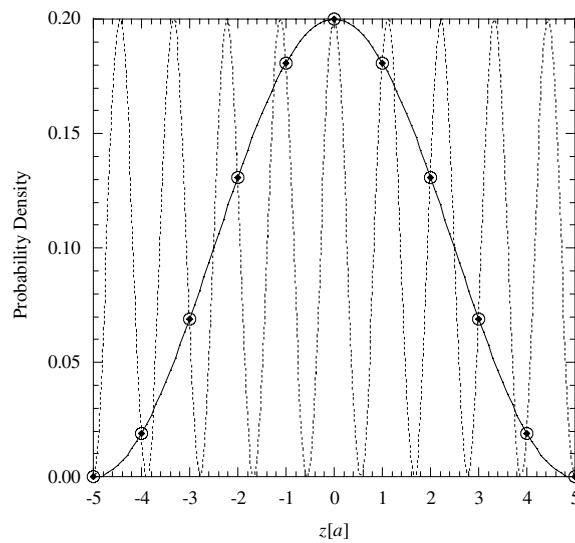


Figure 4. Probability densities of states 1 and 9 in the continuous and tight-binding models. In the continuous model, the probability density is defined throughout the well and is plotted with solid (state 1) and dotted (state 9) lines. In the tight-binding model, the probability density is defined only at the atomic sites and is indicated by solid diamonds (state 1) and open circles (state 9). Note that these densities exactly coincide.

3. Conclusions

The continuous and discrete versions of the Schrödinger equation have distinctly different behaviour. While this difference may be attributed to the mathematical properties of the finite-size mesh spacing, this viewpoint misses much of the physics of the discretized model. Instead, it is more interesting to view the finite mesh spacing as the separation between atoms in a simple tight-binding model. The periodic (as opposed to perfectly parabolic) band and finite bandwidth are then seen to be consequences of the inter-atomic Hamiltonian matrix element. The periodic dispersion of the bulk model likewise explains the finite number of bound states even when confinement is due to infinite-height barriers. Without this perspective, one is left with only the purely mathematical explanation for the finite number of bound states: the finite number of basis orbitals.

Acknowledgments

It is a pleasure to acknowledge discussions with Mark Friesen and Sue Coppersmith. At UAH this work was supported by ARDA through a subcontract from the Jet Propulsion Laboratory. The work described in this publication was carried out in part at the Jet Propulsion Laboratory, California Institute of Technology under a contract with the National Aeronautics and Space Administration. Funding was provided under grants from ARDA, ONR, JPL and NSF (grant No ECC-0228390).

Appendix

Here we recast the tight-binding Schrödinger equation in order to obtain the propagation factors for bulk states. We first use this formulation to derive the boundary conditions under

perfect confinement, equation (17), from the requirement that the applied potential $U \rightarrow \infty$ in the barriers. Next, we show that the bulk dispersion in the well, equation (11), implies the Bloch relation $C_{j\pm 1} = e^{\pm ika} C_j$.

To derive the perfect-confinement boundary conditions, note that within the barriers, $|n| \geq (N+1)$, the potential is constant $U_n = U$. In these regions, rearrange equation (8) and add an identity

$$-V_{ss} C_{n-1} = V_{ss} C_{n+1} + [\varepsilon_s + U - E] C_n \quad (\text{A.1})$$

$$C_n = C_n \quad (\text{A.2})$$

to obtain the generalized eigenproblem [3] (sometimes referred to as the generalized transfer matrix equation) for the single s-orbital per atom chain:

$$\begin{bmatrix} 0 & -V_{ss} \\ 1 & 0 \end{bmatrix} \begin{bmatrix} C_n \\ C_{n-1} \end{bmatrix} = \begin{bmatrix} V_{ss} & (\varepsilon_s + U - E) \\ 0 & 1 \end{bmatrix} \begin{bmatrix} C_{n+1} \\ C_n \end{bmatrix}. \quad (\text{A.3})$$

Equation (A.3) gives the characteristic states (both propagating and evanescent) of the bulk material at a given energy E . The wavefunction of a quantum well bound state for the left barrier, $n \leq -(N+1)$, will be the eigenstate of equation (A.3) which decays as $n \rightarrow -\infty$; for the right barrier, $n \geq N+1$, it will be the eigenstate of equation (A.3) which decays as $n \rightarrow +\infty$. (In a larger model, for example, one having several orbitals per unit cell, the bound-state wavefunction in a barrier region will be a superposition of all eigenstates which decay going farther into the barrier.)

The reverse eigenproblem,

$$C_{j-1} = \lambda_- C_j \quad (\text{A.4})$$

gives the eigenstates in the left barrier. Imposing equation (A.4) on the left-hand side of equation (A.3) yields

$$\lambda_- \begin{bmatrix} 0 & -V_{ss} \\ 1 & 0 \end{bmatrix} \begin{bmatrix} C_{n+1} \\ C_n \end{bmatrix} = \begin{bmatrix} V_{ss} & (\varepsilon_s + U - E) \\ 0 & 1 \end{bmatrix} \begin{bmatrix} C_{n+1} \\ C_n \end{bmatrix}. \quad (\text{A.5})$$

Equation (A.5) is easily rearranged into a homogeneous system which has non-trivial solutions only if its determinant vanishes:

$$\lambda_-^2 + \frac{(\varepsilon_s + U - E)}{V_{ss}} \lambda_- + 1 = 0. \quad (\text{A.6})$$

Note that we explicitly assume $V_{ss} \neq 0$. That is we do not set the matrix element $\langle s; -(N+1)a | \hat{H} | s; -Na \rangle$ to zero to provide confinement in the barriers; the well and barriers are therefore still coupled. Equation (A.6) is readily solved in the limit of large U ; the decaying eigenvalue is

$$\lambda_-^< = \frac{|V_{ss}|}{\varepsilon_s + U - E} + O \left\{ \left(\frac{|V_{ss}|}{\varepsilon_s + U - E} \right)^3 \right\} \quad (\text{A.7})$$

where for the present model we assume $V_{ss} < 0$ and $O\{x^n\}$ denotes corrections to order x^n . Substituting equation (A.7) into equation (A.4) for $j = -N$ and observing that C_{-N} must be finite as it is within the well, we have

$$\lim_{U \rightarrow \infty} C_{-(N+1)} = C_{-N} \lim_{U \rightarrow \infty} \lambda_-^< = 0 \quad (\text{A.8})$$

which is one of the boundary conditions applied in equation (17).

The expansion state for the right-hand barrier is determined in a similar manner. In the right-hand barrier we solve the forward eigenproblem

$$C_{j+1} = \lambda_+ C_j. \quad (\text{A.9})$$

Imposing equation (A.9) on the right-hand side of equation (A.3) and proceeding in the same manner as with equation (A.5), we find that for non-trivial solutions to exist the eigenvalues λ_+ must satisfy

$$\lambda_+^2 + \frac{(\varepsilon_s + U - E)}{V_{ss}} \lambda_+ + 1 = 0. \quad (\text{A.10})$$

We have already solved equation (A.10): the eigenstate which decays going to the right is $\lambda_+^< = \lambda_-^<$ from equation (A.7), so that for $j = N$ and necessarily finite C_N

$$\lim_{U \rightarrow \infty} C_{(N+1)} = C_N \lim_{U \rightarrow \infty} \lambda_+^< = 0. \quad (\text{A.11})$$

We have, therefore, established the right-hand boundary condition (17).

Next, we show that dispersion (11), for a bulk material with $U = 0$, implies that the coefficients satisfy the Bloch relation. Since equations (A.6) and (A.10) are identical, drop the subscript and substitute $E = \varepsilon_s + 2V_{ss}\cos(ka)$ from equation (11), appropriate for a carrier in this band. The quadratic equation now reads

$$\lambda^2 - 2\cos(ka)\lambda + 1 = 0 \quad (\text{A.12})$$

with roots $\lambda^{(\pm)} = e^{\pm ika}$, so that the coefficients for adjacent atoms are related by a phase. Equation (A.12) together with either equations (A.4) or (A.9) thus shows that the coefficients obey the Bloch relation $C_{j\pm 1} = e^{\pm ika} C_j$.

References

- [1] Boykin T B 2001 Tight-binding-like expressions for the continuous-space electromagnetic coupling Hamiltonian *Am. J. Phys.* **69** 793–8
- [2] See, for example, Gasiorowicz S 1974 *Quantum Physics* (New York: Wiley) pp 60–2
- [3] Boykin T B 1996 Generalized eigenproblem method for surface and interface states: the complex bands of GaAs and AlAs *Phys. Rev. B* **54** 8107–15
Boykin T B 1996 Tunnelling calculations for systems with singular coupling matrices: results for a simple model *Phys. Rev. B* **54** 7670–3
- [4] See: Boykin T B, Klimeck G, Eriksson M A, Friesen M, Coppersmith S N, von Allmen P, Oyafuso F and Lee S 2004 Valley splitting in strained silicon quantum wells *Appl. Phys. Lett.* **84** 115–7
- [5] Gradshteyn I S and Ryzhik I M 1994 *Table of Integrals, Series, and Products* 5th edn, ed Alan Jeffry (San Diego, CA: Academic)
- [6] Frensley W R 1994 Quantum transport *Heterostructures and Quantum Devices (VLSI Electronics: Microstructure Science* vol 24) ed W R Frensley and N G Einspruch (San Diego, CA: Academic)
- [7] Lake R, Klimeck G, Bowen R C and Jovanovic D 1997 Single and multiband modelling of quantum electron transport through layered semiconductor devices *J. Appl. Phys.* **81** 7845–69
- [8] Boykin T B, van der Wagt J P A and Harris J S Jr 1991 Tight-binding model for GaAs/AlAs resonant-tunnelling diodes *Phys. Rev. B* **43** 4777–84
- [9] Bowen R C, Klimeck G, Lake R, Frensley W R and Moise T 1997 Quantitative resonant tunnelling diode simulation *J. Appl. Phys.* **81** 3207–13